# The Dynamics and Mechanics of Endothelial Cell Spreading

Cynthia A. Reinhart-King,* Micah Dembo,† and Daniel A. Hammer*
*Department of Bioengineering and Institute for Medicine and Engineering, University of Pennsylvania, Philadelphia, Pennsylvania; and †Department of Biomedical Engineering, Boston University, Boston, Massachusetts

ABSTRACT Cell adhesion to extracellular matrix is mediated by receptor-ligand interactions. When a cell first contacts a surface, it spreads, exerting traction forces against the surface and forming new bonds as its contact area expands. Here, we examined the changes in shape, actin polymerization, focal adhesion formation, and traction stress generation that accompany spreading of endothelial cells over a period of several hours. Bovine aortic endothelial cells were plated on polyacrylamide gels derivatized with a peptide containing the integrin binding sequence RGD, and changes in shape and traction force generation were measured. Notably, both the rate and extent of spreading increase with the density of substrate ligand. There are two prominent modes of spreading: at higher surface ligand densities cells tend to spread isotropically, whereas at lower densities of ligand the cells tend to spread anisotropically, by extending pseudopodia randomly distributed along the cell membrane. The extension of pseudopodia is followed by periods of growth in the cell body to interconnect these extensions. These cycles occur at very regular intervals and, furthermore, the extent of pseudopodial extension can be diminished by increasing the ligand density. Measurement of the traction forces exerted by the cell reveals that a cell is capable of exerting significant forces before either notable focal adhesion or stress fiber formation. Moreover, the total magnitude of force exerted by the cell is linearly related to the area of the cell during spreading. This study is the first to monitor the dynamic changes in the cell shape, spreading rate, and forces exerted during the early stages (first several hours) of endothelial cell adhesion.

## INTRODUCTION

During processes such as tissue regeneration and wound healing, cell adhesion, spreading, and migration are controlled by receptor-mediated interactions with the extracellular matrix (ECM). The synergy among soluble growth factors, cytokines, and the extracellular matrix acts to regulate changes in cell shape, growth, proliferation, and motility (1–5). The interaction between a cell and its substrate has a specific, important ability to control cell morphology via traction exerted through cellular receptors onto the ECM (6). However, little is understood about how the initial interaction between a cell and extracellular matrix results in the generation of traction forces during spreading.

The initial contact between a cell and the ECM is mediated by the adhesion of the cell to the extracellular matrix via integrin receptors present on the cell surface (7). Integrin-ligand binding is followed by the extension of pseudopodia from the cell body. As the cell begins to flatten against the substrate, it forms additional bonds with the ECM, rearranging its cytoskeleton to form actin bundles and focal adhesions (8). To spread, a cell must exert force against its membrane and its substrate to allow for pseudopodial extension and the stabilization of nascent contacts. The resultant net force is a balance between the extensional and contractile forces exerted by the cytoskeletal machinery (6). This balance of forces and the resultant degree of spreading, in part, controls cell physiology. The size of cellular extensions determine the number of adhesions between the cell and ECM molecules, thereby increasing the degree of signaling initiated by the ECM to the cell. Additionally, protrusive forces mediate migration by propelling a cell forward. Likewise, cell contraction is essential for migration, as it allows for the release of the rearward portion of the cell as the cell moves forward (9–11). Cell contraction also aids in the remodeling of the extracellular milieu of the cell, as cellular forces have been shown to align fibronectin and collagen fibrils (12). The balance of extensional and contractile forces that mediate processes such as cell migration and ECM remodeling are thought to also control the dynamic changes in cell spreading that occur when an initially spherical cell flattens against a surface; thus, an examination of cell spreading should inform us about the basic mechanisms of cell-substrate interactions.

Several other studies have investigated the process of cell spreading (13–16). Recently, Dubin-Thaler and co-workers studied the dynamics, but not the mechanics, of cell spreading (14). For very short times (~30 min), they tracked the spreading of fibroblasts on different densities of fibronectin. They found that fibroblasts tend to spread anisotropically, and that there was a lag time in the initiation of spreading that decreased with increasing fibronectin concentration. They also showed that over this time period, the extent of spreading increased with fibronectin density.

Although this study done by Dubin-Thaler et al. addressed some intriguing dynamic features of the early stages of spreading, we sought to extend the work by simultaneously studying the entire time course of spreading (up to 4 h after

*Submitted October 11, 2004, and accepted for publication March 24, 2005.*
Address reprint requests to Daniel A. Hammer, Dept. of Bioengineering, University of Pennsylvania, 3320 Smith Walk, 120 Hayden Hall, Philadelphia, PA 19104. Tel.: 215-573-6761; E-mail: hammer@seas.upenn.edu.

0006-3495/05/07/676/14 $2.00
doi: 10.1529/biophysj.104.054320

initial contact) and the mechanics of spreading during this period. To this end, we used traction force microscopy (TFM) to measure the forces exerted by bovine aortic endothelial cells (BAECs) during spreading on flexible, RGD-derivatized polyacrylamide substrata. The mechanics of endothelial cell spreading are of particular interest to our laboratory not only for comparison to those previously published (17), but also for a better understanding of endothelial cell adhesion and its role in blood vessel formation. By using a well-defined substrate containing the RGD peptide fragment of full-length fibronectin, the synergistic effects of cryptic sites along the full-length fibronectin that are revealed due to cell adhesion and contraction are eliminated. In this way, we have designed a simple, well-defined system to study the mechanics and dynamics of endothelial cell spreading.

Our study of the forces generated during endothelial cell spreading will allow us to address a key issue in cell substrate mechanics—the relationship between focal adhesion formation and stress generation. Techniques similar to traction force microscopy have been used to quantify the forces exerted by cells constrained to micropatterned ECM-coated islands (18) and the traction stresses at focal adhesions (19,20). Balaban and co-workers largely conclude that forces generated by a cell are wholly attributable to the size and number of focal adhesions, whereas Tan and co-workers report a bimodal relationship between contact area and force, where force and contact area are related for areas greater than 1 $\mu m^2$ and those adhesions smaller than 1 $\mu m^2$ appear to exert large forces that do not correlate to size. Similarly, Wang and co-workers have shown that force generation is more likely attributable to nascent focal adhesions, which are generally smaller than 1 $\mu m^2$, at the front of migrating cells (21). In our previous studies using TFM to investigate the traction forces exerted by well-spread endothelial cells, we found that changes in the density of ligand on the substrate lead to changes in cell area, and the total amount of force exerted by the cell on its substrate is directly correlated with the cell's area (17). Our previous results, in combination with the results of others, imply that the force/area relationship found in our experiments is coincidental with the expansion of focal adhesions as area increases. The study presented here directly addresses this issue by measuring forces exerted by cells during the process of spreading, before stress fiber and significant focal adhesion formation.

## MATERIALS AND METHODS

### Cell culture

BAECs were maintained at 37°C and 5% $CO_2$ in Dulbecco's Modified Eagle's Media (Bio-Whittaker, Walkersville, MD) supplemented with 10% calf serum, 0.5% penicillin-streptomycin, and 1% 200 mM L-glutamine (GibcoBRL, Gaithersburg, MD). Cells media was changed every other day, and approximately every seven days the cells were replated to $7.5 \times 10^5$ cells per 75 $mm^2$ flask using trypsin-EDTA (0.05% Trypsin and 0.53 mM EDTA-4Na, GibcoBRL). All experiments were performed with cells between passages 3–9.

Before all spreading experiments, cells were replated sparsely on tissue culture-treated polystyrene dishes. Eight hours later, the cells were serum-starved in DMEM supplemented with 0.5% penicillin-streptomycin and 1% 200 mM L-glutamine for 15 h. After serum-starvation, the cells were replated for experimentation.

### Surface preparation

Coverslips (No. 1, 45 × 50 mm, Fisher Scientific, Pittsburgh, PA) were chemically activated in preparation for covalent attachment of polyacrylamide sheets using the method adapted from the protocol described by Wang and Pelham (22). Briefly, the coverslips were passed through the flame of a Bunsen burner, coated with a thin layer of 0.1 N NaOH and allowed to dry. A layer of 3-aminopropyltrimethoxysilane (200 $\mu$l, Sigma-Aldrich Chemical, St. Louis, MO) was coated on the coverslips, incubated, and repeatedly bathed in distilled water followed by a 30-min incubation in 0.5% glutaraldehyde (70% aqueous stock solution, Sigma-Aldrich Chemical) in phosphate-buffered saline (Invitrogen, Carlsbad, CA) at room temperature. The coverslips were rinsed thoroughly with distilled water and air-dried horizontally, overnight, in a fume hood.

### Synthesis of the bifunctional linker

N-6-((acryloyl)amino)hexanoic acid (N-6) was synthesized using the method described by Pless et al. (23). The N-6 copolymerizes in the acrylamide to form a reactive polyacrylamide gel. The N-6 contains an *n*-succinimidyl ester that is displaced by a primary amine to link the amine-containing ligand to the polyacrylamide substrates.

### Gel synthesis

Gels were prepared using 5% acrylamide (40% w/v solution), 0.1% *n*,*n*′-methylene-bis-acrylamide (2% w/v solution), *n*′-tetramethylethylene diamine, and ammonium persulfate from Bio-Rad Laboratories (Hercules, CA). Additionally, the gels contained 54 mM HEPES, 20 $\mu$mol/ml of N-6 dissolved in ethanol, 2:25 volume of carboxylate-modified fluorescent latex beads (0.5 $\mu$m Fluospheres, Molecular Probes, Eugene, OR), and 1:2000 volume of *n*′-tetramethylethylene diamine. The pH of the monomer solution was adjusted to 6.0 with 3.0 N HCl, the solution was degassed and a 1:200 volume of 10% ammonium persulfate was added. Twenty microliters of the solution was dispensed onto the activated coverslips and the drop was flattened using a circular coverslip (No. 1, 22-mm diameter, Fisher Scientific, Pittsburgh, PA). The entire assembly was turned upside-down and incubated at room temperature for 60 min, allowing polymerization to occur. The circular coverslip was removed and the gel was rinsed in ice-cold DI water for 10 min. This protocol produces a gel that is 70-$\mu$m thick, with a Young's modulus of ~2500 Pa, as described previously (17).

### Covalent attachment of the ligand to the gel

In these experiments, an RGD-containing nonapeptide (with a sequence of $NH_2$-Tyr-Ala-Val-Thr-Gly-Arg-Gly-Asp-Ser-OH) was covalently linked to the polyacrylamide gels. The gels were removed from the DI water and incubated in a 50 mM HEPES (pH 8.0) solution containing peptide. The gel was rinsed with DI water and the unreacted linker capped with ethanolamine. The gels were rinsed with ice-cold DI water and stored at 4°C in DI water.

The peptide density is measured using a solution of 5N NaOH to hydrolyze the amide linkage between the peptide and the acrylamide surface. The concentration of peptide released into solution is determined by comparing its absorbance at 280 nm to that of standard solutions. The density of

peptide on the surface of the gel can be approximated by converting the overall concentration of the peptide within a volume of gel to a surface density of ligand by assuming a 1-nm penetration depth into the gel in which a cell can bind the peptide. The density of ligand on the surface of the gel in these experiments ranges from ~150 to 1500 mol/$\mu m^2$.

## Cell spreading

Cells were pretreated as described above and replated into Leibovitz L-15 media (Invitrogen, Carlsbad, CA) supplemented with 10% calf serum, 0.5% penicillin-streptomycin, and 1% 200 mM L-glutamine. The cells were plated at a density of 5500 cells/$cm^2$ onto polyacrylamide gels and immediately placed onto an Olympus Inverted I×70 Microscope stage (Olympus America, Melville, NY) in a chamber maintained 37°C for observation. Images of the cells were taken periodically and later analyzed for cell area and perimeter using Scion Image software (Scion, Frederick, MD). The light path contains a green monochromatic IF-550 filter (Olympus America) to minimize light damage to the cells.

## Traction force microscopy of spreading cells

Traction force microscopy has been described previously (10). Briefly, traction forces were determined based on deformations in the polyacrylamide substrate relative to the relaxed substrate as detected by movements of 0.5-$\mu$m beads embedded in the gel. Phase contrast images of the cell were taken periodically during spreading. Directly after a phase image was taken, a corresponding fluorescent image of the beads embedded beneath the cell was taken. At the end of 4 h of spreading, the cell was removed using trypsin-EDTA and an image of the beads in their unstressed state was captured. Using custom-written software, the bead displacements within the gel were calculated, the cell and nucleus outlines were drawn, and a mesh that fits within the outline of the cell was created. Using the bead displacements and the material properties of the gel, the most likely surface traction vectors were calculated using the technique described by Dembo and Wang (10).

The overall force, $|F|$, exerted by the cell on its substrate, is an integral of the traction field magnitude over the area, $|F| = \int\int \sqrt{(T_x^2(x,y)+T_y^2(x,y)}dxdy$, where $\mathbf{T}(x,y) = [T_x(x,y), T_y(x,y)]$ is the continuous field of traction vectors defined at any spatial position $(x,y)$ within the cell.

## Immunostaining of focal adhesions and stress fibers

BAECs were plated sparsely on tissue culture-treated polystyrene dishes for 8 h before 15 h of serum-starvation in DMEM supplemented with 0.5% penicillin-streptomycin and 1% 200 mM L-glutamine. After serum-starvation, the cells were replated in standard media on polyacrylamide gels conjugated with an RGD-containing peptide. At various time points, the cells were fixed in 2% paraformaldehyde, followed by permeabilization using 0.2% Triton X-100. The samples were each blocked using 10% goat serum (Sigma Aldrich Chemical) and stained with either Alexa546-labeled phalloidin (Molecular Probes) or murine anti-vinculin monoclonal antibody (Upstate Cell Signaling Solutions, Charlottesville, VA) followed by AlexaFluor 488 conjugated goat anti-mouse IgG secondary antibody (Molecular Probes). The phalloidin-stained actin was visualized using an Olympus Inverted IX70 Microscope with an Olympus 60×, NA 0.7, phase objective and images were gathered using a SPOT RT Slider Camera (Diagnostic Instruments, Sterling Heights, MI). F-actin polymerization was quantified by calculating the average fluorescence intensity of a population of cells after background subtraction. Focal adhesions were visualized using an Olympus Inverted I×81 Microscope with an Olympus 20×, NA 0.60 objective and images were gathered using a Cooke Sensicam QE camera (Cooke, Auburn Hills, MI) (generously provided by Dr. Michael King, University of Rochester, Rochester, NY).

# RESULTS

## Density of ligand mediates the rate and extent of spreading

We monitored BAECs for adhesion and shape changes after trypsinization and replating on polyacrylamide gels derivatized with various concentrations of a peptide containing the ligand-binding sequence RGD over a period up to 4 h. Images of the cell were taken during spreading and recorded for later analysis (Fig. 1). Because cell-cell contact is known to affect the extent of cell spreading, only those cells that spread without contact with adjacent cells were analyzed.

For each image, cell area was calculated and the results were plotted against time (Fig. 2 *A*). Note that the cell area increases monotonically with time as the cell spreads, reaching a steady state. The data were regressed via a weighted, nonlinear least-squares regression to a modified error function of the form

$$A = \left[erf\left(\frac{t - t_{50}}{\tau}\right) + 1\right] \times A_{50}, \quad (1)$$

where $A$ is the area of the cell, $t$ is the time after plating, $t_{50}$ is the time at which the cell has spread to half its maximum, and $A_{50}$ is half the maximum area of the cell. The best-fit model parameters at each concentration are shown in Table 1. The appearance of the data suggest such a form rather than a simple exponential function, since it allows for the possibility of a lag before the initiation of spreading as was suggested by Dubin-Thaler et al. (14). Additionally, based on the experimental data in Fig. 2 *A*, an early inflection point is evident, a feature lacking in a simple exponential function.

As shown previously (17) and as seen in Fig. 2 *A*, the area increases with increasing peptide concentration. To better elucidate this relationship, Fig. 2 *B* plots $A_{50}$, the half-maximal area, versus the peptide concentration. When plotted on a semi-log scale, $A_{50}$ and the concentration of peptide are linearly related and can be closely fit to the equation

$$A_{50} = 347 \times \ln\left(\frac{c}{c_0}\right), \quad (2)$$

where $c$ is the concentration of peptide and $c_0$ has a value of $1.86 \times 10^{-4}$ mg/ml, where the slope ranges from 270 to 417 $\mu m^2$ within a 95% confidence interval. Additionally, the parameters calculated, based on the phenomenological relationship from Eq. 1, indicate that there is also a relationship between the *rate* of spreading and the concentration of peptide, contrary to that previously suggested by Dubin-Thaler and co-workers (14) that spreading rate is independent of ligand density. We find that

$$k_{max} = \left(\frac{dA}{dt}\right)_{t_{50}} = 6.14 \times \left(\frac{c}{c_0}\right)^{0.28}, \quad (3)$$

where $k_{max}$ is the maximum rate of spreading. From least-squares linear regression, the exponent of the power-law ranges from 0.27 to 0.294 $\mu m^2$/min within a 95% confidence interval.

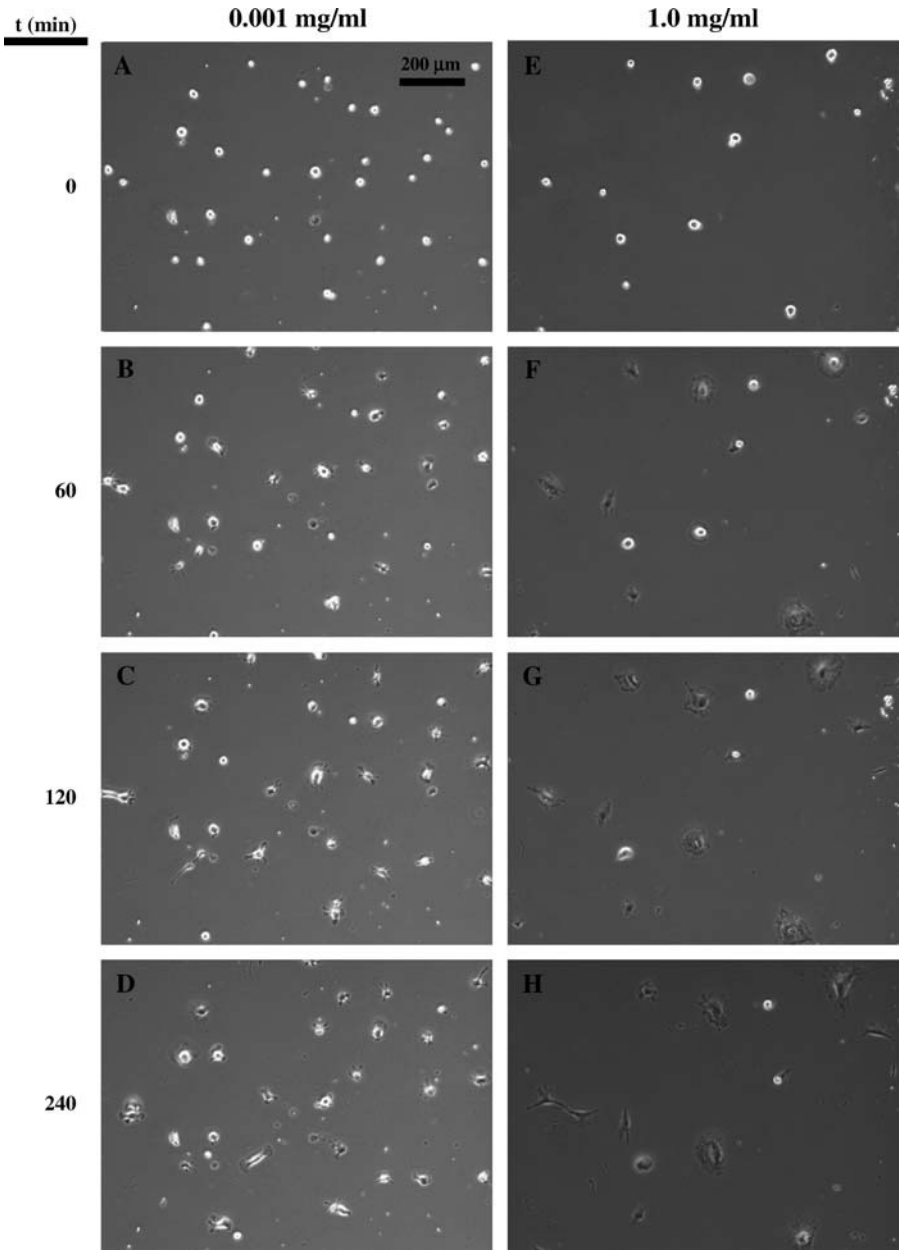


FIGURE 1 The effect of ligand density on BAEC morphology during spreading. BAECs were plated on polyacrylamide gels containing varying amounts of RGD-containing peptide and observed under 10× magnification during spreading. Representative images from the highest and lowest densities of peptide are shown here. Cell area was significantly reduced on 0.001 mg/ml of peptide (*A–D*), in comparison to cells on 1.0 mg/ml of peptide (*E–H*). *A* and *E* are taken at time equal to 0; *B* and *F* are taken at time equal to 1 h; *C* and *G* are taken at time equal to 2 h; and *D* and *H* are taken at time equal to 4 h.

In addition to calculating the area of the cell, we investigated changes in the perimeter of the cell in response to spreading. Plotting the changes in perimeter with respect to changes in area on a log-log plot (Fig. 3) reveals a power-law relationship of the form

$$\tilde{P} = \alpha \tilde{A}^{\beta}, \tag{4}$$

where $\tilde{P}$ is the dimensionless perimeter of the cell ($P/P_0$), $\tilde{A}$ is the dimensionless area of the cell ($A/A_0$), and $\alpha$ and $\beta$ are presented in Table 2. On a log-log scale, $\tilde{P}$ is linear with $\tilde{A}$, and the slope is characterized by $\beta$. The physical significance of $\beta$ is illustrated in Fig. 4 for two distinct limits of spreading. First consider the growth of a cell maintaining an approximately circular outline, a phenomenon that can be referred to as isotropic spreading (Fig. 4 *A*). In this case, the $\beta$-exponent approaches 0.5, and a quadrupling in cell area corresponds to a doubling of the cell perimeter. This is in contrast to the spreading of a spindlelike cell with many thin extensions, so-called ''anisotropic'' spreading (Fig. 4 *B*). In this case, the exponent $\beta$ approaches 1 in the limit of thin extensions. As the pseudopod thickness increases, $\beta$ falls between 0.5 and 1, with larger pseudopods leading to smaller values of $\beta$ approaching 0.5. Therefore, by investigating the relationship between area and perimeter during spreading in this manner and quantifying $\beta$, we have been able to quantify the mode of spreading as a function of ligand density. Data

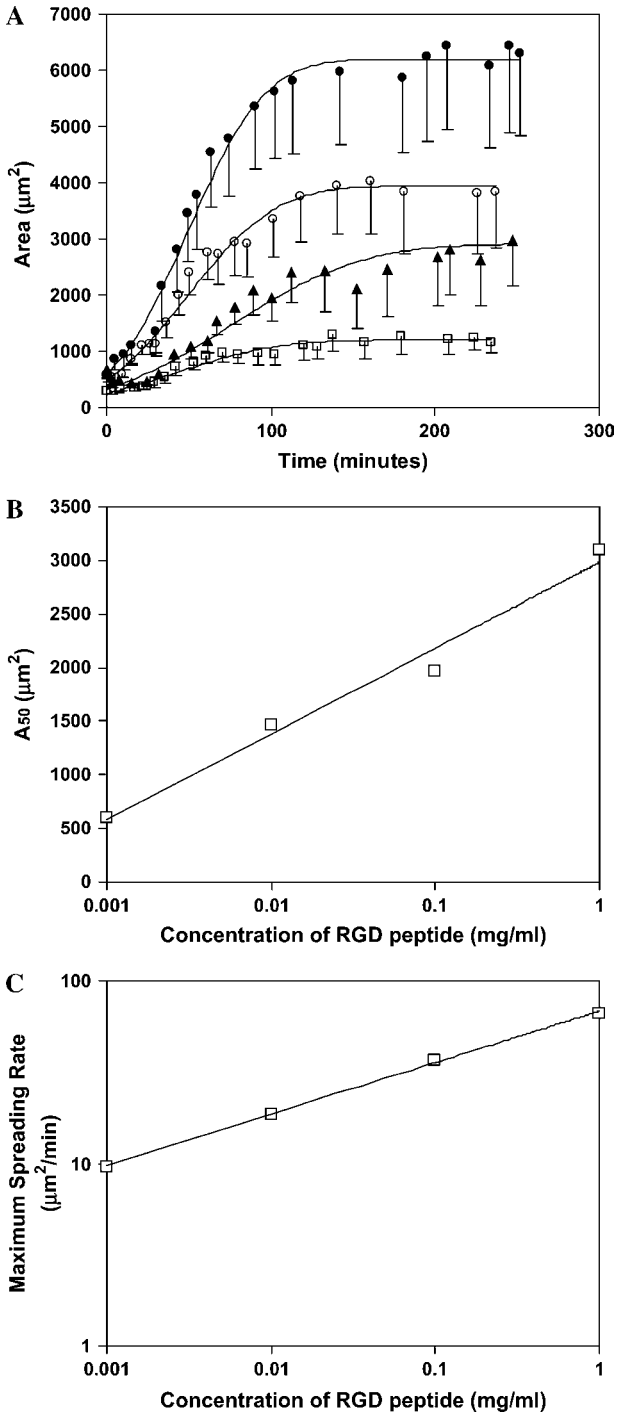


FIGURE 2 Ligand density controls the maximum area and spreading growth rate of spreading BAECs. (*A*) BAECs were plated on polyacrylamide gels containing varying amounts of RGD-containing peptide and the area of the cell was quantified and plotted against time. The results are fit to a modified error function as described in the text. (●) 1.0 mg/ml, (○) 0.1 mg/ml, (▲) 0.01 mg/ml, and (□) 0.001 mg/ml. Error bars represent mean ± SE of nine cells. (*B*) The area at half-maximum, as determined from the model regression in *A*, was plotted against the concentration of ligand on the gel, indicating a linear relationship between the log of the ligand concentration and the area of the cell. (*C*) The maximum growth rate, as determined from the model regression in *A*, was plotted against the concentration of ligand on the gel, revealing a log-linear relationship.

**TABLE 1 Regression parameter values for data presented in Fig. 2**

| Ligand concentration (mg/ml) | $t_{50}$ (min) | $A_{50}$ ($\mu m^2$) | $\tau$ (min) | $k_{max}$ ($\mu m^2$/min) | $k_{initial}$ ($\mu m^2$/min) | $R^2$ |
|---|---|---|---|---|---|---|
| 0.001 | 40.6 | 606 | 71.1 | 9.62 | 7.08 | 0.994 |
| 0.01 | 75.5 | 1460 | 89.0 | 18.5 | 9.22 | 0.985 |
| 0.1 | 48.8 | 1970 | 60.2 | 36.9 | 19.8 | 0.997 |
| 1.0 | 48.8 | 3100 | 52.6 | 66.5 | 29.4 | 0.999 |

regression indicates that at higher densities of ligand, the average behavior of a cell is isotropic, where the cell spreads while maintaining a circular morphology, as indicated by the values of $\beta$ in Table 2. This is in contrast to the behavior at lower densities of ligand where the cell spreads anisotropically by extending numerous pseudopodia.

Using the cell area and perimeter, we define a shape factor, $f$, as the ratio of the perimeter of the cell to the area of the cell. This parameter has units of 1/length, and is useful in characterizing the relative number of extensions per unit length. To better understand this parameter, consider the case of an ideal, isotropically spreading cell maintaining its circular morphology, as depicted in Fig. 4 *A*. The plot of the ratio of perimeter/area against time is continually decreasing, and in the limit where $r$ gets larger the ratio of perimeter/area becomes small. In Fig. 5, the average shape factor, $f$, of spreading cells was plotted against time for four different ligand densities. The data is well fit by a nonlinear damped oscillator model,

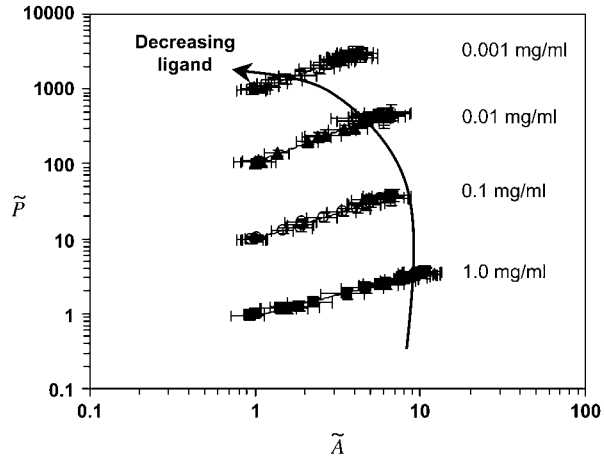


FIGURE 3 Ligand density controls the mode of spreading. BAECs were plated on polyacrylamide gels containing varying amounts of RGD-containing peptide and the area and perimeter of the spreading cells was quantified. The perimeter is related to the area through a power law as detailed in the text and the exponent of the power law changes with ligand density. (●) 1.0 mg/ml, (○) 0.1 mg/ml, (▲) 0.01 mg/ml, and (□) 0.001 mg/ml. Each successive ligand concentration, in decreasing order, is shifted up one decade from the next highest ligand concentration for visual clarity. Error bars represent the mean ± SE of nine cells.

**TABLE 2 Regression parameters for power law model relating cell perimeter to area presented in Fig. 3**

| Ligand concentration (mg/ml) | $\alpha$ | $\beta$ | $R^2$ |
|---|---|---|---|
| 0.001 | 0.97 | 0.77 | 0.989 |
| 0.01 | 1.04 | 0.82 | 0.99 |
| 0.1 | 0.99 | 0.69 | 0.993 |
| 1.0 | 0.94 | 0.55 | 0.995 |

$$f = 0.09 \times \left|\sin\left[\frac{2\pi}{260}t + \frac{\pi}{2}\right]\right| \times e^{-\omega_d t} + f_\infty, \qquad (5)$$

where $f$ is the shape factor, $t$ is time, $\omega_d$ is the damping coefficient, and $f_\infty$ is the steady-state value of the shape factor. Each of the four data sets in Fig. 5 is fit to this model and the resulting parameter values are presented in Table 3. Notably, the model is a two-parameter fit where the oscillation amplitude (0.09 $\mu m^{-1}$), the natural frequency ($2\pi/260$ $min^{-1}$), and the phase shift ($\pi/2$) are conserved over all four ligand concentrations; only $f_\infty$ and $\omega_d$ vary as a function of ligand concentration. The oscillations in the shape factor are prevalent at low ligand densities, but do not exist at higher ligand densities. The negative changes of $f$ with $t$ are indicative of periods where the area is increasing more quickly than the perimeter, which would be consistent with cell spreading to fill regions staked out by earlier pseudopodial extensions. However, increasing values of $f$ versus $A$ indicate the perimeter is increasing more quickly than the area, indicative of pseudopodial extension; the oscillation in $f$ versus $t$ indicates that, at low densities of ligand, there is alternation of pseudopodial extension and periods where the cell body fills in the area between extensions to create a rounder morphology. The damping coefficient increases with the ligand density, indicating that higher ligand densities either, 1), prevent substantial pseudopodial extension before the movement of the rest of the cell body; or either, 2), display a nonsynchronous pseudopodial extension among a population such that the average behavior results in what appears to be relatively isotropic spreading when ensemble-averaged. Based on qualitative observation, it appears that both scenarios contribute to the lack of synchronicity. At high concentrations of peptide, the pseudopodial extension form at random times in the cell population over time, and cells tend to spread more isotropically than on lower densities of peptide.

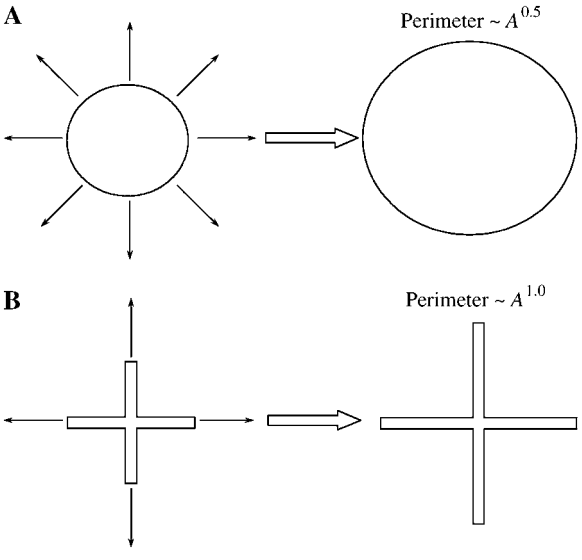


FIGURE 4 (*A*) A schematic diagram of isotropic spreading, where the exponent in the power law equals 0.5. (*B*) A schematic diagram of spreading through radial projections, where the exponent approaches 1.

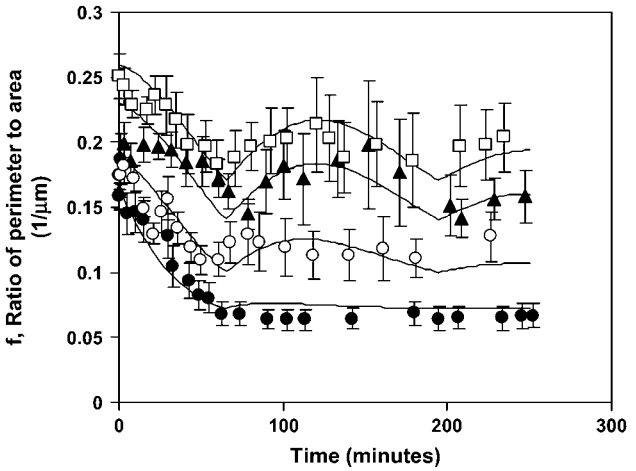


FIGURE 5 The ratio of perimeter/area over time exhibits oscillations at low ligand density. The ratio of perimeter/area was plotted against time for cells spreading on each of the four different ligand concentrations. Error bars represent the mean ± SE of nine cells. The data are fit to a two-parameter damped oscillator model as described in the text. As the amount of ligand increases, the number of oscillations decrease, indicating that ligand may function to support isotropic spreading and prevent pseudopodial extension. (●) 1.0 mg/ml, (○) 0.1 mg/ml, (▲) 0.01 mg/ml, and (□) 0.001 mg/ml.

## Forces exerted during spreading are dependent on cell size and substrate ligand density

Previously, our results showed that after 24 h of incubation on an RGD-derivatized substrate, the total force exerted by the cell onto the substrate is linearly related to the area of the cell (17). Other studies have indicated that the relationship between force and the cell area is actually controlled by the

**TABLE 3 Parameter values for damped oscillator model of cell spreading data presented in Fig. 5**

| Ligand concentration (mg/ml) | $\omega_D$ ($min^{-1}$, × $10^{-3}$) | $f_\infty$ | $R^2$ |
|---|---|---|---|
| 0.001 | 5.21 | 0.17 | 0.7835 |
| 0.01 | 5.83 | 0.14 | 0.3494 |
| 0.1 | 10.40 | 0.10 | 0.7875 |
| 1.0 | 29.20 | 0.0725 | 0.8654 |

size and area of the focal adhesion complexes independent of the cell area (19,20). To further investigate the origin of force generation, we examined the forces exerted by endothelial cells during spreading, before focal adhesion and stress fiber formation. Cells were plated on polyacrylamide gels derivatized with varying densities of RGD and observed during spreading up to a period of 4 h.

Traction force microscopy was used to measure the forces exerted by the cells on its substrate during spreading (Fig. 6). Even at very low concentration of ligand, cells exert significant, detectable traction forces early in spreading. At the earliest stages of spreading, these tractions are uniform and directed inward, at both low and high ligand densities. As the cell begins to spread by extending projections, stresses are concentrated at the pseudopodial tips (Fig. 6, *A–D*). Despite the outward extensions of the membrane, the results presented here indicate that the basal surface of the cell pulls inwardly on the surface in a state of contraction. This same pattern exists in all the cells observed in our study, regardless of the concentration of ligand. Additionally,

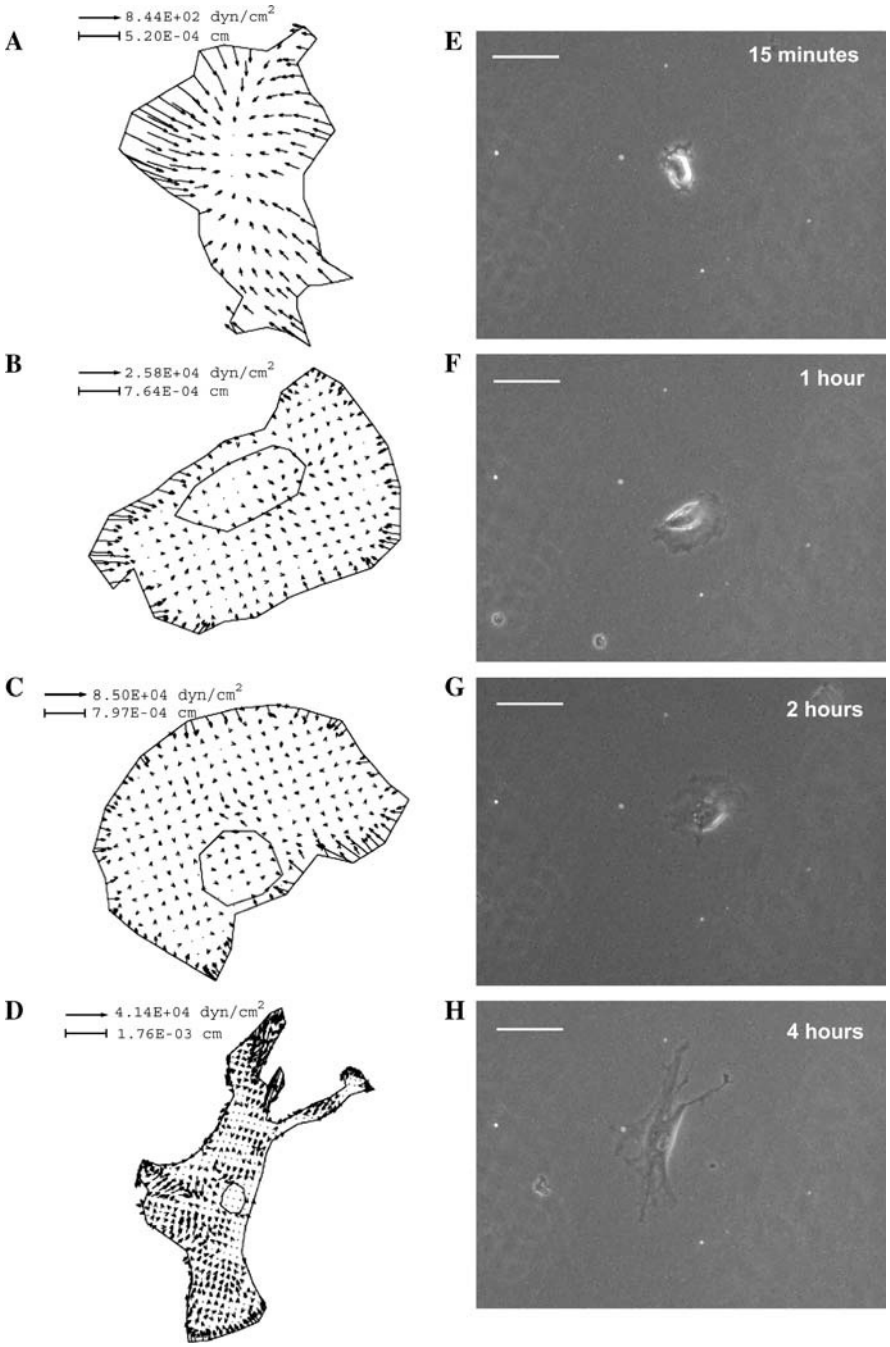


FIGURE 6 Traction forces are evident early in spreading, and typically point inward throughout the entire process of spreading. Forces exerted by a cell during spreading onto its substrate were measured using traction force microscopy. (*A–D*) Traction maps of a representative cell spreading on an intermediate concentration of peptide, 0.1 mg/ml. (*E–H*) Phase-contrast images of those cells pictured in *A–E*. The scale bar in the phase-contrast images is 50 $\mu$m.

strong tractions localized to a given area of the cell are not necessarily predictors of the formation of later pseudopodial extensions. Likewise, early pseudopodial extensions do not necessarily indicate the positions of future extensions.

In addition to investigating the pattern of traction forces, we quantified the overall magnitude of force exerted by the cell. Our results show that the magnitude of force exerted by a spreading cell is linearly related to, but not uniquely determined by, its area (Fig. 7 *A*); however, the magnitude of the force generated is dependent on the density of ligand on the substrate. As the density of ligand increases, the change in force with area increases (indicated by the *slope* of Fig. 7 *A*). Plotting the slope of the regressed lines against the concentration of ligand on a semi-log plot (Fig. 7 *B*) reveals that the force/area slope is log-linear with respect to ligand concentration, best fit to the equation

$$m = 1191.8 \times \ln(1802.6 \times c), \quad (6)$$

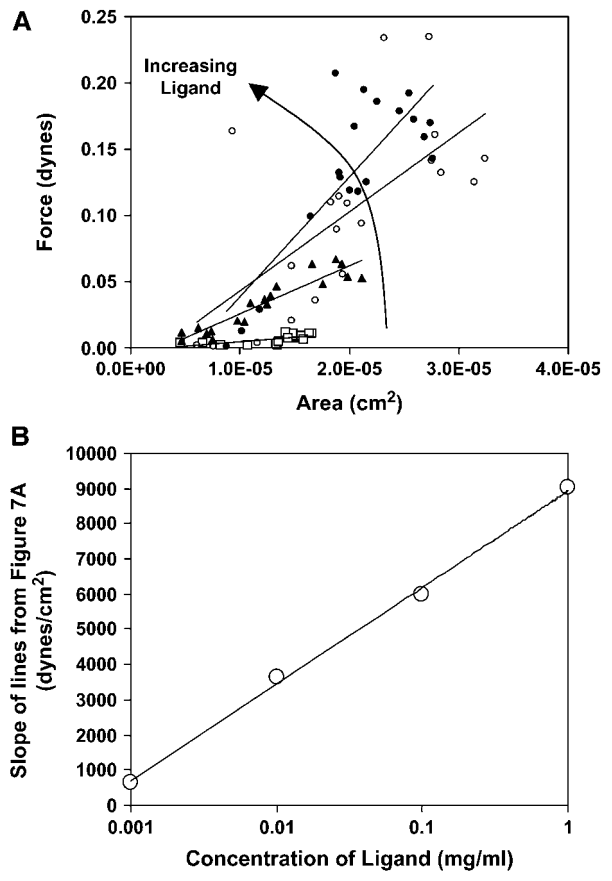


FIGURE 7 Force and area are linearly related during spreading. BAECs were plated on polyacrylamide gels and immediately monitored for traction forces during spreading. Both force and area are monitored over a 4-h time period beginning at the time of plating. (*A*) During the first 4 h of spreading, the force exerted by the cell onto its substrate increases linearly with increasing area. (●) 1.0 mg/ml, (○) 0.1 mg/ml, (▲) 0.01 mg/ml, and (□) 0.001 mg/ml. (*B*) The slope of the regression lines from *A* were plotted against the log of the concentration of ligand, revealing a linear relationship between the two. $R^2$ of the best fit equals 0.998.

where $m$ is the slope of the lines presented in Fig. 7 *A* and the slope resulting from a least-squares linear regression ranges from 1110 to 1270 dyn/cm$^2$ within a 95% confidence interval. Clearly, during the early stages of spreading, force and area are related and the relationship is dependent on ligand concentration. Additionally, we considered the possibility that the total force exerted by the cell is related to the perimeter of the cell; however, no statistically significant dependence was found.

## The generation of traction force precedes stress fiber formation

To better elucidate the molecular mechanisms that control changes in force with respect to the area of a spreading cell, we investigated the time course of actin polymerization and the appearance of stress fibers. Because stress fibers have been shown to be highly contractile (24), we hypothesized that the generation of tractions would correspond to the development of stress fibers. BAECs were pretreated as described above by preplating and serum starvation. The cells were then plated on polyacrylamide gels derivatized with 1.0 mg/ml of RGD-containing peptide. At various times, the cells were fixed and stained using Alexa-546-phalloidin.

The quantity of f-actin was quantified by measuring the total fluorescent intensity of a population of cells at each time (Fig. 8). The total amount of filamentous actin increases during spreading and peaks at ~3 h, and then decreases to a steady-state value by 24 h. As illustrated in Fig. 6, force generation well precedes 3 h. In fact, detectable forces are exerted within 30 min of plating, before any detectable changes in actin polymerization, which we observed to occur ~60 min after plating. Additionally, qualitative examination of the images of Fig. 8 *B* reveals that stress fibers do not appear until ~2–3 h after plating. When compared with the results presented in Fig. 6, these data strongly suggest that cells are capable of exerting significant forces before complete actin polymerization or visible stress fiber formation.

Because actin polymerization peaks at 3 h, we compared the force generation of the spreading cells after 3 h, as described in this study, to the behavior of cells that had been plated for 24 h, as described in our previous study of endothelial force generation (17). When the total force exerted by the cell is plotted against the cell area for every cell over all concentrations studied for $t$ greater than 3 h, force and area again appear to be linearly related (Fig. 9). The slope of this plot is 7.1 $\times$ 10$^3$ dyn/cm$^2$, and is statistically similar to the relationship we found in our previous study of cells that had been plated for 24 h before force measurements (17).

## The generation of traction force precedes focal adhesion formation

Several previous studies have used variations of the traction force microscopy technique described here to measure

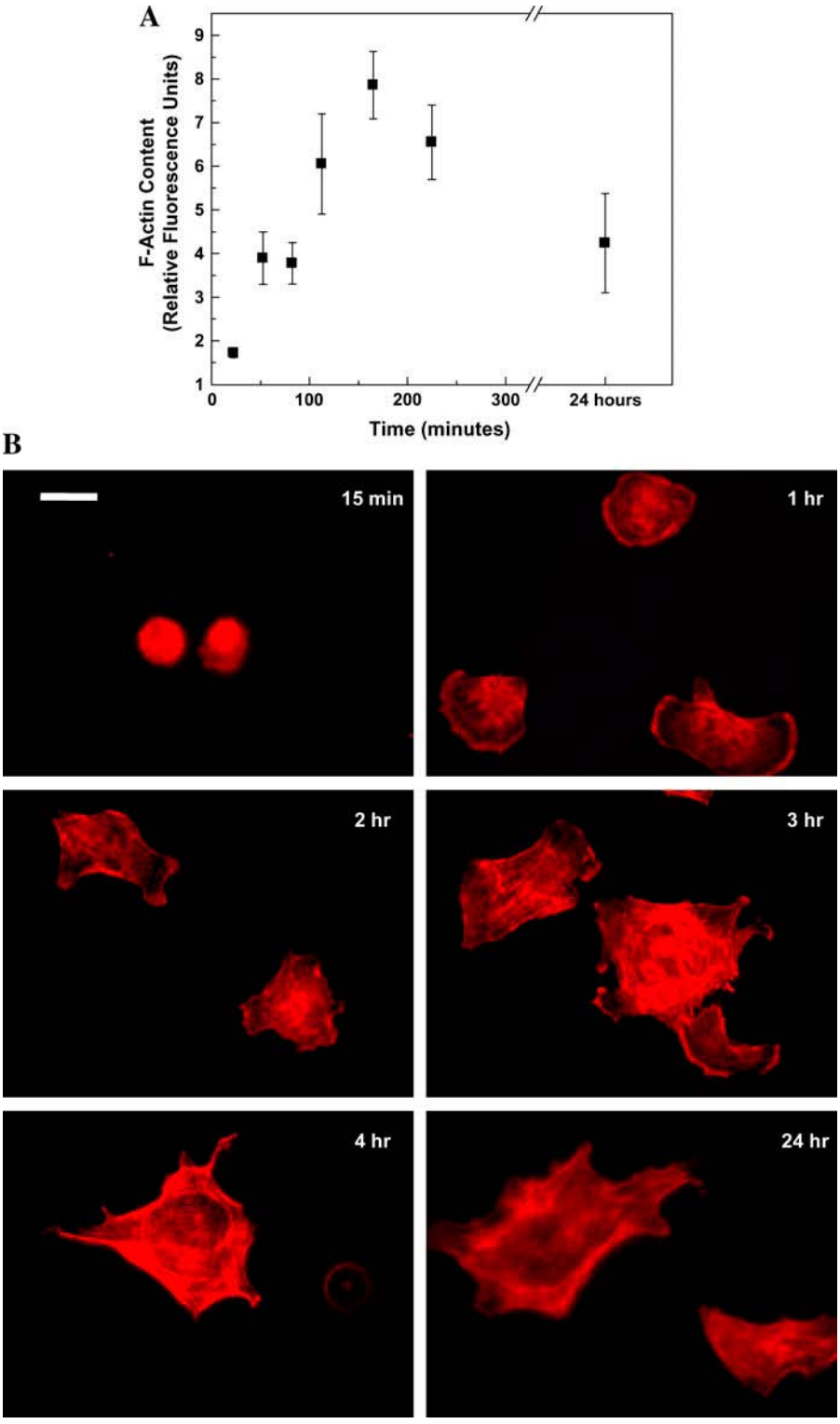


FIGURE 8 Actin polymerization increases during spreading with a maximum at ~3 h. (*A*) Cells were plated on polyacrylamide gels derivatized with 1.0 mg/ml of RGD-containing peptide and fixed at various time points. The cells were stained with Rhodamine-phalloidin, and f-actin content was quantified by comparing relative fluorescence intensities of the cells. Data are plotted with their mean ± SE. Actin polymerization increases with cell spreading and reaches a maximum at ~3 h. By 24 h, the amount of f-actin has decreased to a steady-state value. (*B*) The cells were visualized using fluorescence microscopy at 60× magnification.

traction forces exerted by cells (10,11,19–21,25–27). In some cases, these studies conclude that the forces exerted by the cell originate from focal adhesions (19, 20). We investigated this assumption by looking at the time course of focal adhesion formation relative to the time course for traction force generation.

Vinculin was chosen as a marker for focal adhesion formation (28) because it has been shown to be one of the first intercellular molecules recruited to the sites of focal complexes, precursors to focal adhesions (29). We found that focal adhesions appear at varying times during spreading and depend on the density of ligand on the substrate (Fig. 10).

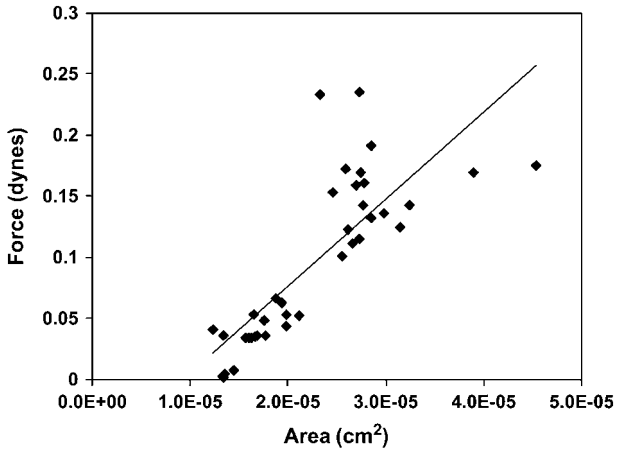


FIGURE 9 The force exerted by cells 3 h after plating on various densities of peptide was plotted against the cell area. The relationship between force and area approaches a steady-state value after complete actin polymerization. Three hours was chosen because it was the time at which actin polymerization peaks and stress fibers are detected. The plot reveals an approximately linear relationship with a slope of 7100 dyn/cm$^2$. This slope is statistically similar to that found within our previous study of the same cells 24 h after plating (17), indicating that stress fibers may dominate the steady-state relationship between force and area found in our previous work.

Before adhesion, vinculin is spread diffusely throughout the cell. In cells plated on the highest density of peptide, vinculin clustering occurs relatively early, between 45 and 60 min. At the two intermediate values of ligand density, vinculin clustering appears between 60 min and 2 h. In cells plated on the lowest density of peptide, there is very little vinculin clustering at all, even at 24 h. Clearly, the number of vinculin clusters and timing of the appearance of the clusters is in part dictated by the density of ligand on the substrate.

Most striking is the ability of the cells to exert significant traction forces before focal adhesion formation. At the highest concentrations of peptide, focal adhesions form relatively quickly, within 1 h, and yet traction forces are evident within minutes after plating (Fig. 6). For example, after only 10 min of plating, cells plated on the highest density of ligand are already exerting 7% of their maximum force. Additionally, cells plated on the lowest ligand density form very few focal adhesions even at 24 h and yet these cells are still capable of exerting significant forces soon after plating. Only 1 h after plating, cells on the lowest ligand density are already exerting 14% of their maximum force. Our data indicate that focal adhesion formation is not necessary for traction generation.

## DISCUSSION

Despite numerous studies of cell spreading, ours is perhaps the first to observe the generation of force in cells during the process of spreading from the state of a completely rounded cell to a completely spread cell. We suspect that one deterrent to these studies is the sensitivity of the cell to the light of the microscope (30). Observation of the full time course of spreading has only been possible when the light is extremely minimized by limiting the light intensity of the bulb in addition to using green and neutral density filters in series. This longer exploration of spreading dynamics allows us to correlate the dynamics of spreading with force and ligand density. Using time-lapse microscopy, immunofluorescence, and traction force microscopy, we have found that:

1. Ligand density increases the rate of spreading.
2. Cells on higher densities of ligand tend to spread isotropically.
3. Cells are capable of exerting organized traction forces before focal adhesion and stress fiber formation.
4. The overall force a cell exerts and its area are related even during spreading.

Several studies have reported a relationship between cell area and ECM density (2,31,32), but here we report that ligand density increases the rate of spreading. In a separate study of cell spreading recently performed by Dubin-Thaler et al., it was concluded that in mouse embryonic fibroblasts, ligand density affects the lag time before cells start to spread, but the rate of spreading is independent of ligand density (14). Our data confirms that the initial rate of spreading is dependent on ligand density; however, in contrast to Dubin-Thaler et al., our data show that, in BAECs, the maximal rate of area growth varies significantly with ligand density. Because Dubin-Thaler et al. and Giannone et al. both waited for the onset of spreading before observing and measuring fibroblast spreading, and only tracked cells for ~35 min, it is possible that we are able to observe changes in cell behavior that they were not able to detect because of their limited observation time. It should be noted that the differences in cell behavior between the study presented here and that of Sheetz and co-workers (14,15) could also be explained by the differences in the cell types investigated.

The changes in cell area with time revealed a monotonic increase to a plateau in cell area. The data was fit to an error function, which successfully incorporates all of the features of the curves and fits all four data sets (Fig. 2 *A*). The error function itself is interesting, in that it represents the integral of a normal distribution (Fig. 11). The derivative of our data may be thus interpreted as a normal distribution of some cellular event over time. We can only speculate on the nature of these events, but we suspect that it is the binding of integrin and ligand. At early time points, the binding of ligand is minimal, but increases with time as the cell spreads. At some later point during spreading, the majority of integrin molecules are bound and it becomes less likely that a new bond will form, thus leading to a decrease in new integrin ligation. Thus, integrin ligation may very well give rise to the changes in area observed.

By investigating the changes in area and perimeter during spreading, we have established a simple quantitative basis

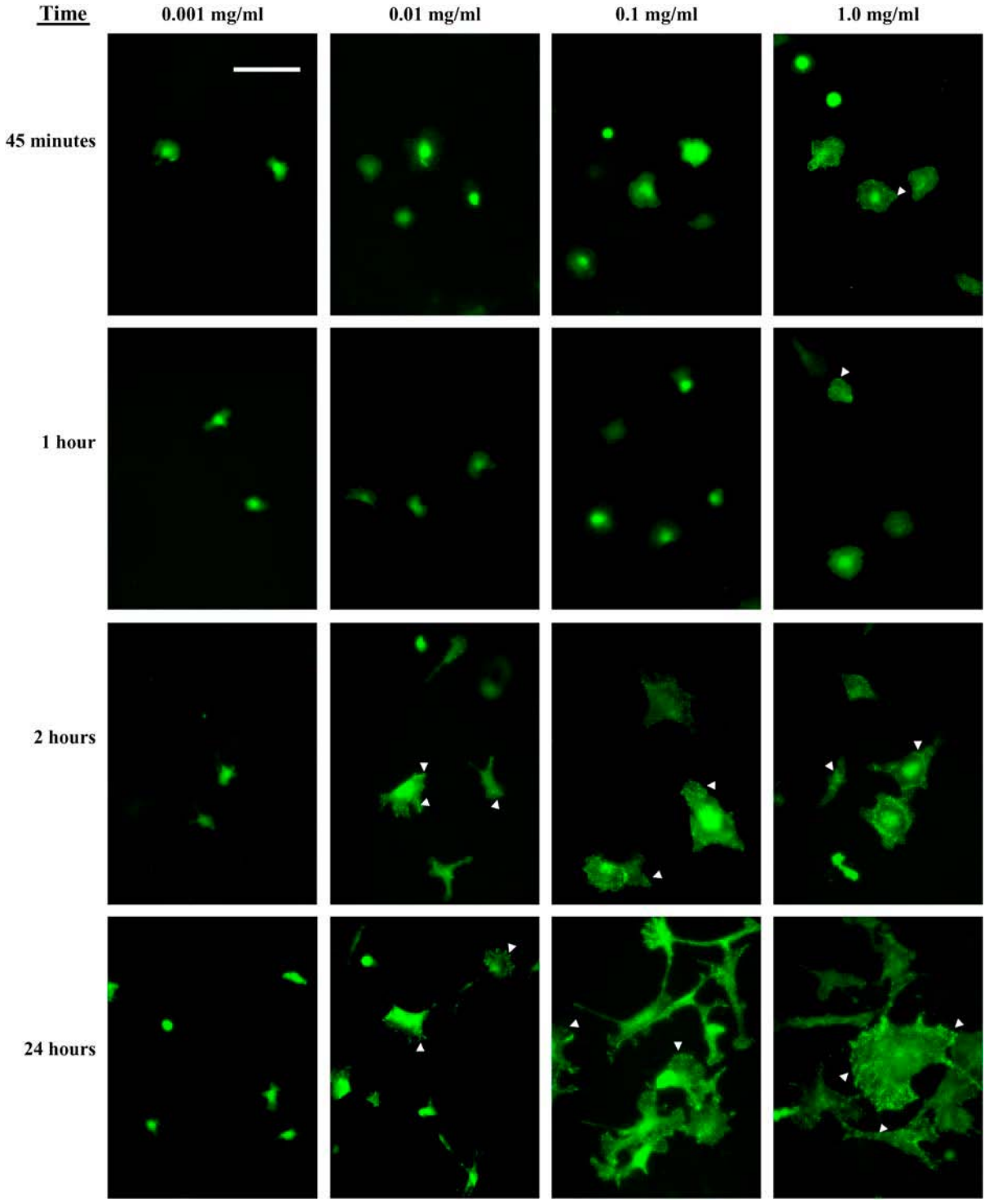


FIGURE 10 Focal adhesions, indicated by arrowheads, form sooner on higher densities of peptide. BAECs were plated on polyacrylamide gels derivatized with varying concentration of RGD-containing peptide. At various times after plating, the cells were fixed and stained with an anti-vinculin antibody and a secondary fluorescein-conjugated antibody. The cells were then visualized at 20× magnification. Focal adhesions form much more rapidly and are much more numerous at higher concentrations of peptide. On the lowest concentration of peptide, very few focal adhesions are visible even at 24 h. The scale bar is 100 $\mu$m.

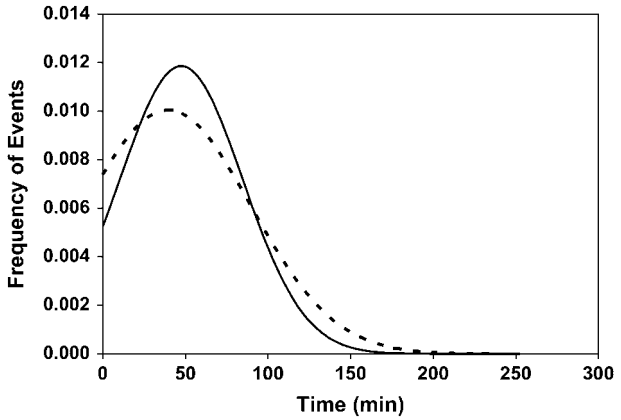


FIGURE 11 Changes in area over time during spreading are mediated by a Gaussian distribution of cell-substrate binding events. Because the changes in cell area over time during spreading can be fit to the error function, the derivative of the regression analysis to Fig. 2 was taken, illustrating a Gaussian distribution of events over time during spreading. The distribution for the highest (1.0 mg/ml, *solid line*) and the lowest (0.001 mg/ml, *dashed line*) are presented. We hypothesize that these events are the net number of binding events between receptor and substrate ligand. In this scenario, binding is most likely to occur when the cell is sufficiently spread to contact a large area of ligand, forming new bonds, but before an increase in the number of breakage events.

for comparing the modes of cell spreading; more complicated methods were recently employed by Sheetz and coworkers (14,15), as they tracked changes in cell radius at evenly spaced points along the circumference of a cell. The power law relationship that exists between perimeter and area indicates that cells on higher densities of ligand spread isotropically, whereas cells on lower densities of peptide are more likely to spread anisotropically (Fig. 3). Dubin-Thaler et al reported that isotropic spreading is most prevalent in serum-deprived cells (14). During serum-deprivation, membrane receptors are not occupied by the growth factors often found in serum, and therefore are more available for binding with substrate-bound ligand. Likewise, when the cell encounters high densities of ligand, as was tested in the experiments presented here, the balance toward soluble-ligand bound receptors and substrate-ligand bound receptors shifts toward the binding of the receptors to the substrate. The number of substrate-ligand bound receptors may, in fact, determine the threshold between isotropic and anisotropic spreading.

Our investigation into the dynamics of cell spreading includes a comparison of the changes in cell shape that accompany changes in cell area. We defined a parameter, called the shape parameter, $f$, as the ratio of perimeter/area. The shape parameter is a measure of the approximate number of pseudopodia per unit length for a population of cells. At low concentrations of peptide, the spreading behavior of cells ($f$ versus $A$) oscillates between periods of area increasing more quickly than the perimeter and periods of the perimeter increasing more quickly than the area. This oscillation implies that cells on a lower density of peptide, spread by a cycle of extending pseudopodia, followed by a general increase in the cell body in concert over a population. At higher densities of peptide, there are no oscillations and the shape parameter indicates that the cells are spreading isotropically. Perhaps the increased ligand density acts as the damper represented in our model, preventing significant pseudopodial extension. The comparison of obtained damping coefficients may indicate that at lower densities of peptide, the cell is able to send out extensions more readily, since the membrane is less tightly bound to the substrate, whereas at higher densities of ligand, the cell is so firmly bound it can only spread in a pancakelike manner. A similar behavior occurs during cell migration (29,33,34), where a cell can be so tightly bound at high densities of ECM that it does not send out the extensions necessary for motility, yet at low densities a cell sends out filopodia to sense its substrate and the filopodia become the foundation for the extension of a lamellipodium.

The oscillations seen in Fig. 5 occur even though the shape factor is a result of an average over the perimeter of each cell and an average over many cells. These observations are distinct from results recently published by Dubin-Thaler et al. who reported that over a small section of cell perimeter, the radius increases in stochastic, transient extension periods (STEPs) (14). In that study, the steps are described for individual sections along the perimeter of a cell and persist for $<1$ min, whereas our study shows that over the cell population the duration of the oscillations last over many minutes. For the oscillations described here and that of Dubin-Thaler et al. to be representative of the same phenomenon, this would imply that the subcellular oscillations of the Dubin-Thaler et al. study are somehow synchronized between cells and perhaps within a single cell. Such a cooperative behavior was not revealed by the single cell studies of Dubin-Thaler et al. (14).

Cells can exert forces early on in spreading, before any significant stress fiber or focal adhesion formation. The magnitude of these forces is comparable to those exerted by the cell at later times. Our results are the first to show the presence of traction forces without the presence of focal adhesions. Several studies have shown that small nascent focal adhesions are capable of forces greater than those measured for mature focal adhesions (19,21); therefore we cannot rule out the possibility that there exist small nascent focal adhesions in our spreading cells that we are unable to detect. An additional study done by Galbraith et al. found that adhesion between an ECM-ligand-coated bead and integrin receptors gain the ability to exert measurable forces upon maturation into focal complexes, as marked by the recruitment of vinculin (29), indicating that mechanical force applied to the cell stimulates the strengthening of adhesions through the recruitment of vinculin. In contrast, we show that the initial adhesions formed between the cell and its substrate are sufficiently strong to exert measurable traction forces

before the detection of vinculin clustering. Future studies that will lead to a better understanding of focal adhesion formation and traction generation should include additional cell spreading studies that monitor simultaneously for GFP-tagged vinculin and traction force generation. Ultimately, the systematic monitoring of real-time recruitment of fluorescently tagged focal adhesion proteins to adhesion sites in conjunction with the use of TFM will lead to critical insights into the molecular mechanisms of traction generation.

In addition to exerting forces early in adhesion, a spreading cell displays an organized distribution of forces. These forces all appear to be directed inward toward the cell center, despite the movements of the cell membrane outward. This general pattern of traction forces has been reported before in migratory fibroblasts (35), indicating a ubiquitous feature of force generation, likely controlled by the fundamental nature of spreading and contractility in cells. The key difference between migration and spreading, however, is that in spreading, all portions of the membrane tend to be extending, and there is no clear direction for the cell. Thus, the lamellipod-pseudopod asymmetry commonly seen in migration does not seem to exist in spreading; however, the modes of membrane extension and force generation appear to be similar.

Previously, we showed that in cells that have been plated for 24 h, given adequate time to spread and form focal adhesions, traction forces are proportional to the area of the cell (17). Knowing that focal adhesions are the points of contact between a cell and the substrate and that the number of focal adhesions increase with area (36), one might conclude that the relationship between the force exerted by the cell and the area of the cell is, in fact, a relationship between the force exerted by the cell and the total number, or individual size, of focal adhesions. However, the results presented here indicate that total force exerted during spreading is proportional to the cell area before significant focal adhesion formation. Therefore, it is possible that vinculin clustering is not necessary for traction generation.

The existence of forces before the appearance of focal adhesions or stress fibers is intriguing for several reasons. These data may indicate that other techniques used to measure forces by assuming that all forces originate from focal adhesions may be neglecting forces produced elsewhere across the membrane-ECM interface. Note significant force generation has occurred before focal adhesion formation, even when comparing to systems where ultimately strong forces are exerted at steady state. Clearly, this suggests that individual integrin-ligand bonds can transmit force before clustering into focal complexes.

The authors thank Nastaran Zahir and Dr. William Marganski for technical assistance, and Drs. Ingrid Sarelius and Richard Waugh for helpful discussions and use of equipment.

The work was funded in part by National Institutes of Health grants No. HL64388 to D.A.H. and No. GM61806 to M.D., and a Whitaker Graduate Fellowship to C.A.R.

## REFERENCES

1. Zhu, X., and R. K. Assoian. 1995. Integrin-dependent activation of MAP kinase: a link to shape-dependent cell proliferation. *Mol. Biol. Cell.* 6:273–282.
2. Ingber, D. E. 1990. Fibronectin controls capillary endothelial cell growth by modulating cell shape. *Proc. Natl. Acad. Sci. USA.* 87:3579–3583.
3. Asthagiri, A. R., C. A. Reinhart, A. F. Horwitz, and D. A. Lauffenburger. 2000. The role of transient ERK2 signals in fibronectin- and insulin-mediated DNA synthesis. *J. Cell Sci.* 113:4499–4510.
4. Gospodarowicz, D., and G. M. Lui. 1981. Effect of substrata and fibroblast growth factor on the proliferation in vitro of bovine aortic endothelial cells. *J. Cell. Physiol.* 109:69–81.
5. McAuslan, B. R., V. Bender, W. Reilly, and B. A. Moss. 1985. New functions of epidermal growth factor: stimulation of capillary endothelial cell migration and matrix dependent proliferation. *Cell Biol. Int. Rep.* 9:175–182.
6. Lauffenburger, D. A., and A. F. Horwitz. 1996. Cell migration: a physically integrated molecular process. *Cell.* 84:359–369.
7. Hynes, R. O. 1987. Integrins: a family of cell surface receptors. *Cell.* 48:549–554.
8. Burridge, K., K. Fath, T. Kelly, G. Nuckolls, and C. Turner. 1988. Focal adhesions: transmembrane junctions between the extracellular matrix and the cytoskeleton. *Annu. Rev. Cell Biol.* 4:487–525.
9. Maheshwari, G., and D. A. Lauffenburger. 1998. Deconstructing (and reconstructing) cell migration. *Microsc. Res. Tech.* 43:358–368.
10. Dembo, M., and Y. L. Wang. 1999. Stresses at the cell-to-substrate interface during locomotion of fibroblasts. *Biophys. J.* 76:2307–2316.
11. Galbraith, C. G., and M. P. Sheetz. 1997. A micromachined device provides a new bend on fibroblast traction forces. *Proc. Natl. Acad. Sci. USA.* 94:9114–9118.
12. Tranquillo, R. T., M. A. Durrani, and A. G. Moon. 1992. Tissue engineering science: consequences of cell traction force. *Cytotechnology.* 10:225–250.
13. de Hoog, C. L., L. J. Foster, and M. Mann. 2004. RNA and RNA binding proteins participate in early stages of cell spreading through spreading initiation centers. *Cell.* 117:649–662.
14. Dubin-Thaler, B. J., G. Giannone, H. G. Dobereiner, and M. P. Sheetz. 2004. Nanometer analysis of cell spreading on matrix-coated surfaces reveals two distinct cell states and STEPs. *Biophys. J.* 86: 1794–1806.
15. Giannone, G., B. J. Dubin-Thaler, H. G. Dobereiner, N. Kieffer, A. R. Bresnick, and M. P. Sheetz. 2004. Periodic lamellipodial contractions correlate with rearward actin waves. *Cell.* 116:431–443.
16. Wakatsuki, T., R. B. Wysolmerski, and E. L. Elson. 2003. Mechanics of cell spreading: role of myosin II. *J. Cell Sci.* 116:1617–1625.
17. Reinhart-King, C. A., M. Dembo, and D. A. Hammer. 2003. Endothelial cell traction forces on RGD-derivatized polyacrylamide substrata. *Langmuir.* 19:1573–1579.
18. Parker, K. K., A. L. Brock, C. Brangwynne, R. J. Mannix, N. Wang, E. Ostuni, N. A. Geisse, J. C. Adams, G. M. Whitesides, and D. E. Ingber. 2002. Directional control of lamellipodia extension by constraining cell shape and orienting cell tractional forces. *FASEB J.* 16:1195–1204.
19. Tan, J. L., J. Tien, D. M. Pirone, D. S. Gray, K. Bhadriraju, and C. S. Chen. 2003. Cells lying on a bed of microneedles: an approach to isolate mechanical force. *Proc. Natl. Acad. Sci. USA.* 100: 1484–1489.
20. Balaban, N. Q., U. S. Schwarz, D. Riveline, P. Goichberg, G. Tzur, I. Sabanay, D. Mahalu, S. Safran, A. Bershadsky, L. Addadi, and B. Geiger. 2001. Force and focal adhesion assembly: a close relationship studied using elastic micropatterned substrates. *Nat. Cell Biol.* 3:466–472.
21. Beningo, K. A., M. Dembo, I. Kaverina, J. V. Small, and Y. L. Wang. 2001. Nascent focal adhesions are responsible for the generation

of strong propulsive forces in migrating fibroblasts. *J. Cell Biol.* 153:881–888.

22. Wang, Y. L., and R. J. Pelham, Jr. 1998. Preparation of a flexible, porous polyacrylamide substrate for mechanical studies of cultured cells. *Methods Enzymol.* 298:489–496.
23. Pless, D. D., Y. C. Lee, S. Roseman, and R. L. Schnaar. 1983. Specific cell adhesion to immobilized glycoproteins demonstrated using new reagents for protein and glycoprotein immobilization. *J. Biol. Chem.* 258:2340–2349.
24. Katoh, K., Y. Kano, and K. Fujiwara. 2000. Isolation and in vitro contraction of stress fibers. *Methods Enzymol.* 325:369–380.
25. Oliver, T., K. Jacobson, and M. Dembo. 1998. Design and use of substrata to measure traction forces exerted by cultured cells. *Methods Enzymol.* 298:497–521.
26. Shiu, Y. T., S. Li, W. A. Marganski, S. Usami, M. A. Schwartz, Y. L. Wang, M. Dembo, and S. Chien. 2004. Rho mediates the shear-enhancement of endothelial cell migration and traction force generation. *Biophys. J.* 86:2558–2565.
27. Wang, H. B., M. Dembo, and Y. L. Wang. 2000. Substrate flexibility regulates growth and apoptosis of normal but not transformed cells. *Am. J. Physiol. Cell Physiol.* 279:C1345–C1350.
28. Geiger, B., K. T. Tokuyasu, A. H. Dutton, and S. J. Singer. 1980. Vinculin, an intracellular protein localized at specialized sites where microfilament bundles terminate at cell membranes. *Proc. Natl. Acad. Sci. USA.* 77:4127–4131.
29. Galbraith, C. G., K. M. Yamada, and M. P. Sheetz. 2002. The relationship between force and focal complex development. *J. Cell Biol.* 159:695–705.
30. McKenna, N. M., and Y. L. Wang. 1989. Culturing cells on the microscope stage. *Methods Cell Biol.* 29:195–205.
31. Gaudet, C., W. A. Marganski, S. Kim, C. T. Brown, V. Gunderia, M. Dembo, and J. Y. Wong. 2003. Influence of type I collagen surface density on fibroblast spreading, motility, and contractility. *Biophys. J.* 85:3329–3335.
32. Truskey, G. A., and T. L. Proulx. 1993. Relationship between 3T3 cell spreading and the strength of adhesion on glass and silane surfaces. *Biomaterials.* 14:243–254.
33. Palecek, S. P., J. C. Loftus, M. H. Ginsberg, D. A. Lauffenburger, and A. F. Horwitz. 1997. Integrin-ligand binding properties govern cell migration speed through cell-substratum adhesiveness. *Nature.* 385: 537–540.
34. DiMilla, P. A., K. Barbee, and D. A. Lauffenburger. 1991. Mathematical model for the effects of adhesion and mechanics on cell migration speed. *Biophys. J.* 60:15–37.
35. Munevar, S., Y. L. Wang, and M. Dembo. 2001. Distinct roles of frontal and rear cell-substrate adhesions in fibroblast migration. *Mol. Biol. Cell.* 12:3947–3954.
36. Chen, C. S., J. L. Alonso, E. Ostuni, G. M. Whitesides, and D. E. Ingber. 2003. Cell shape provides global control of focal adhesion assembly. *Biochem. Biophys. Res. Commun.* 307:355–361.